Supplementary Information for

Guest Solvent-Directed Isomeric Metal–Organic Frameworks for the Kinetically Favorable Separation of Carbon Dioxide and Methane

Dan Lai [a,#], Fuqiang Chen [a,#], Lidong Guo [a], Lihang Chen [a], Jie Chen [a], Qiwei Yang [a,b], Zhiguo Zhang [a,b], Yiwen Yang [a,b], Qilong Ren [a,b], Zongbi Bao [a,b,*]

[a] *Key Laboratory of Biomass Chemical Engineering of the Ministry of Education, College of Chemical and Biological Engineering, Zhejiang University, Hangzhou 310027, China*

[b] *Institute of Zhejiang University–Quzhou, Quzhou 324000, China*

* Corresponding author.

E-mail address: baozb@zju.edu.cn (Z. Bao).

[#] These authors contributed equally to this work.

X-ray diffraction analysis

Powder X-ray diffraction (PXRD) patterns of the samples were collected on an X'Pert diffractometer (PANalytical, the Netherlands) using Cu Kα emission radiation (λ = 0.154 nm) at a range of 5 °–40 °(2θ angle range) with a step size of 0.02 ° per second. The scanning electron microscope was measured on a Hitachi SU-8010 (Hitachi, Japan). The thermal gravimetric analysis (TGA) was examined from 50 to 800 ℃ on a Pyris 1 TGA instrument (Perkin-Elmer) under a nitrogen atmosphere at a constant heating rate of 10 ℃·min^{-1}.

The single-crystal X-ray diffraction of the as-synthesized crystal was performed at 173 K using a Burker Smart Apex II diffractometer with graphite-monochromated Cu Kα radiation. The structure was solved by direct methods using SHELXTL [1] program and refined by full-matrix least-squares methods with SHELXL.

Heat of adsorption calculations

The Clausius–Clapeyron equation and Langmuir method are used to calculate the isosteric heat of adsorption (Q_{st}). It defined as:

$$Q_{\mathrm{st}} = -RT\left(\frac{\partial \ln P}{\partial T}\right)_{n_{\mathrm{a}}} \quad \text{(S1)}$$

where n_a (mmol·g^{-1}) is the amount of adsorbed gas, T (K) is the temperature, P (kPa) is the pressure, Q_{st} (kJ·mol^{-1}) is the isosteric heat of adsorption. Integration of the equation gives:

$$\ln P = \frac{Q_{\mathrm{st}}}{RT} + C \quad \text{(S2)}$$

The heat of adsorption at a given uptake was calculated from the slopes of the isosteres according to the equations as mentioned. The fitting parameters of Langmuir–Freundlich model were displayed in Tables S3–S5.

Dynamic selectivity calculations

The kinetic selectivity can be defined as the ratio of the two gases' diffusion time constants. Diffusion time constants (D_c/r_c^2) were calculated by the short-time solution of the diffusion equation assuming a step-change in the gas-phase concentration with the following micropore diffusion model [2]. The microporous adsorbent particle exposed to a step-change in sorbate concentration at the external surface of the particle at time zero. Heat transfer is assumed to be sufficiently rapid, relative to the sorption rate.

$$\frac{m_t}{m_\infty} \approx \frac{6}{\sqrt{\pi}}\sqrt{\frac{D_c t}{r_c^2}} - 3\frac{D_c t}{r_c^2} \quad \left(\frac{m_t}{m_\infty} < 0.85\right) \quad \text{(S3)}$$

where D_c is the intracrystalline diffusivity, m_t is the adsorbed at time t, m_∞ is the adsorbed amount at equilibrium, and r_c is the radius of the equivalent spherical particle.

Combined selectivity calculations

The combined selectivity was calculated based on equlibrium selectivity and kinetic selectivity using the following equations:

$$\beta_{12} = \frac{D_1}{D_2} \quad \text{(S4)}$$

$$S_{12} = \alpha_{12} \times \sqrt{\beta_{12}} \quad \text{(S5)}$$

where D_1 and D_2 are diffusion time constants of component 1 and component 2, β_{12} is the kinetic selectivity, and α_{12} is the kinetic selectivity.

Diffusion activation energy calculations.

Temperature-dependent diffusion time constants used to calculate the diffusion activation energy using the Arrhenius equation, which is given by

$$\frac{D_c}{r_c^2} = k_A \exp\left(\frac{-E_a}{RT}\right) \quad \text{(S6)}$$

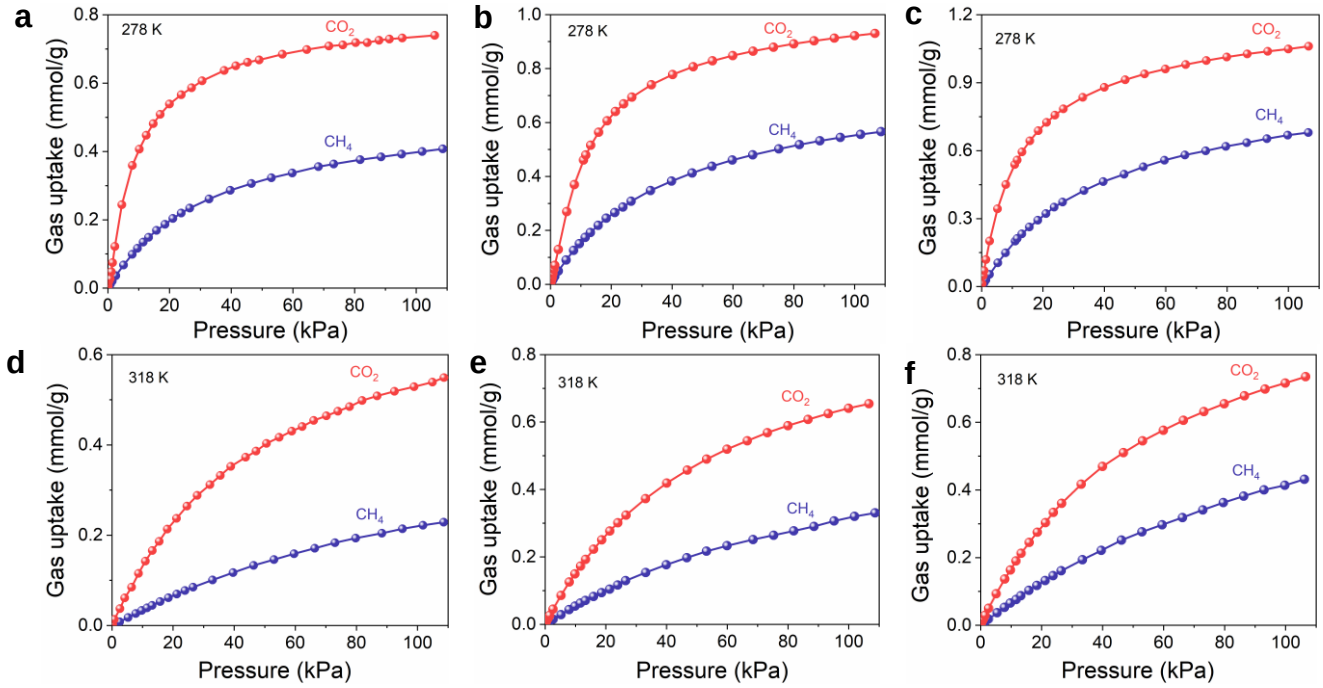

Fig. S1. Adsorption isotherms of CO_2 and CH_4 at 278 and 318 K on (a, d) CuFMOF-a, (b, e) CuFMOF-b, and (c, f) CuFMOF-c.

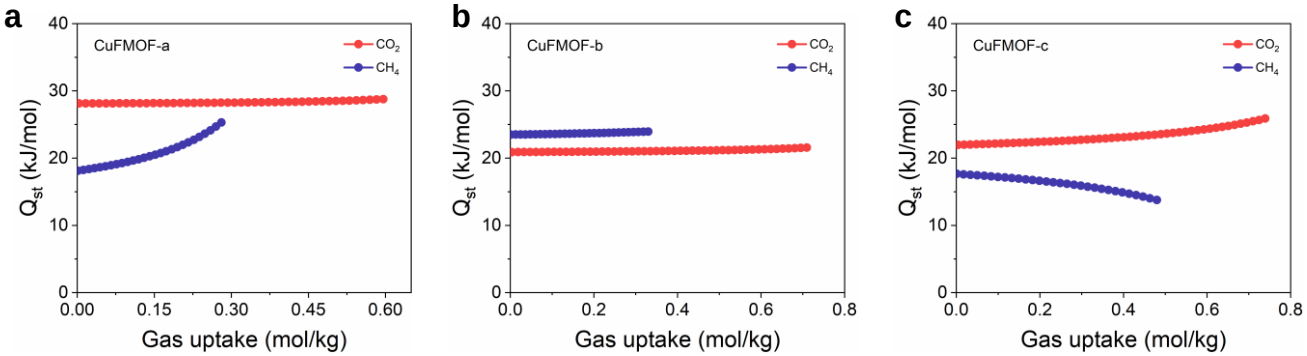

Fig. S2. Isosteric heat of adsorption calculated for CO_2 and CH_4 on (a) CuFMOF-a, (b) CuFMOF-b, and (c) CuFMOF-c based on Clausius–Clapeyron equation.

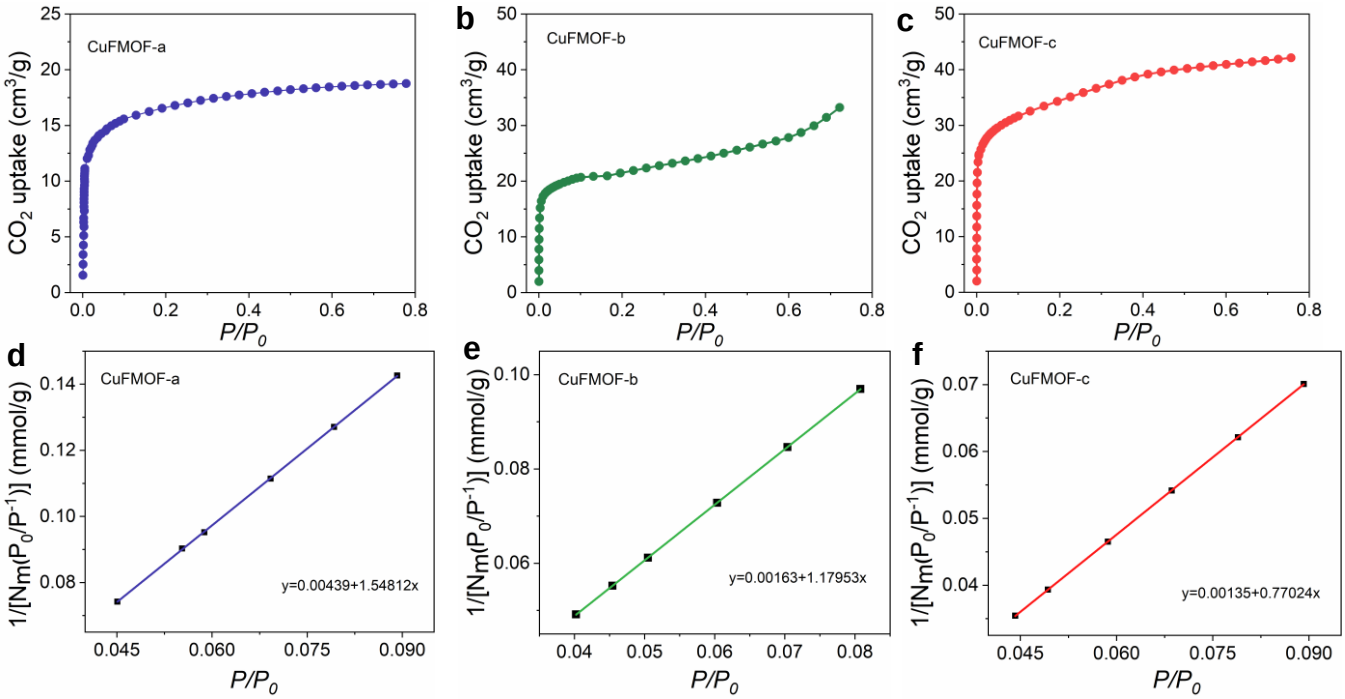

Fig. S3. CO_2 adsorption isotherms at 195 K and the corresponding fitting lines for (a, d) CuFMOF-a, (b, e) CuFMOF-b, and (c, f) CuFMOF-c.

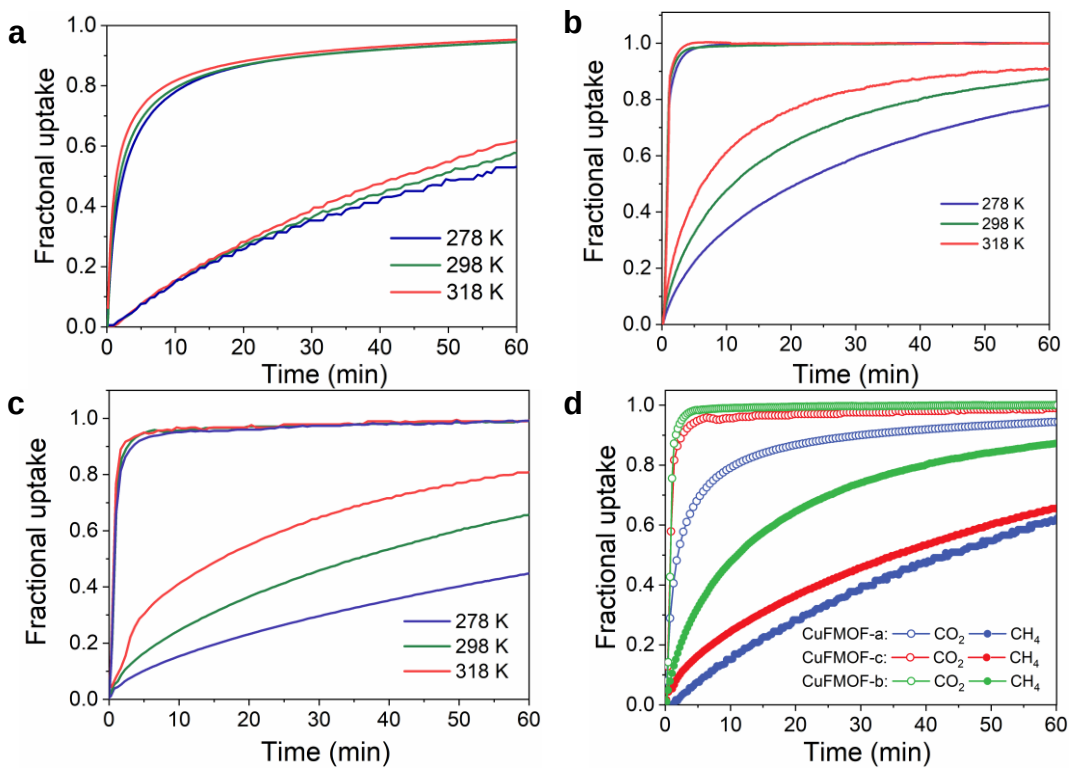

Fig. S4. Fractional adsorption profiles of CO_2 (top) and CH_4 (bottom) at 278, 298, and 318 K on the (a) CuFMOF-a, (b) CuFMOF-b, and (c) CuFMOF-c and (d) fractional adsorption gas uptake profiles of CO_2 and CH_4 for CuFMOF-a (blue), CuFMOF-c (red) and CuFMOF-b (green) at 298 K.

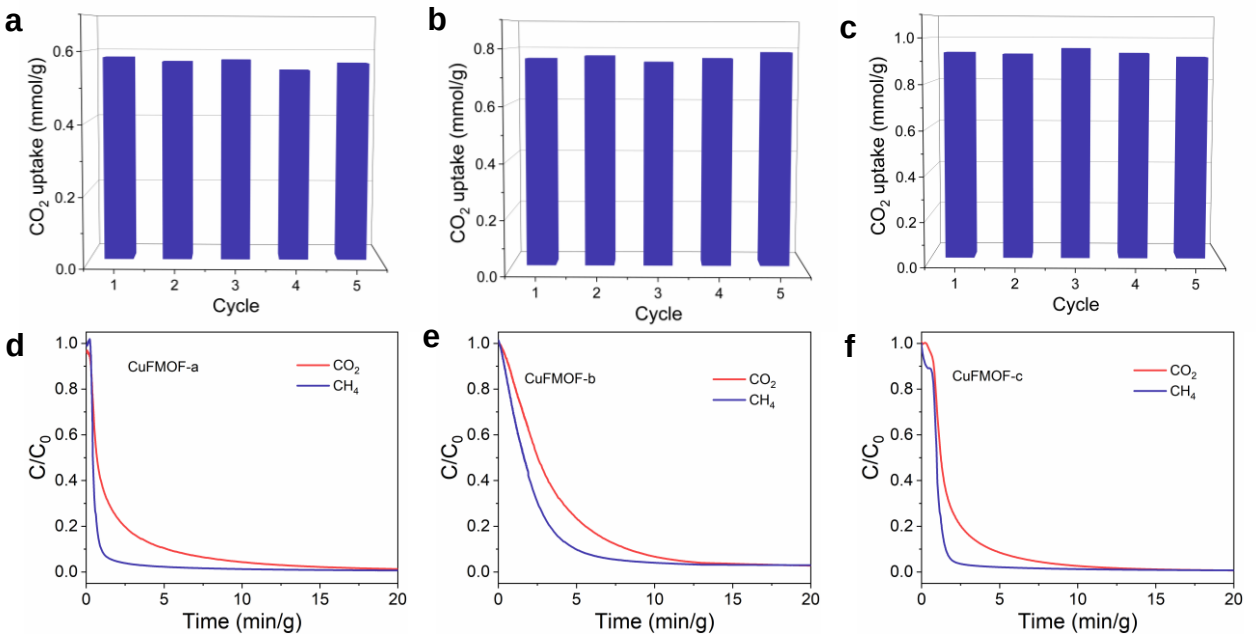

Fig. S5. Cycling performance of breakthrough experiments for (a) CuFMOF-a, (b) CuFMOF-b, and (c) CuFMOF-c and experimental desorption curves of CO_2 and CH_4 of (d) CuFMOF-a, (e) CuFMOF-b, and (f) CuFMOF-c under ambient conditions with a constant He rate of 8 $mL \cdot min^{-1}$ at 298 K and 1 bar.

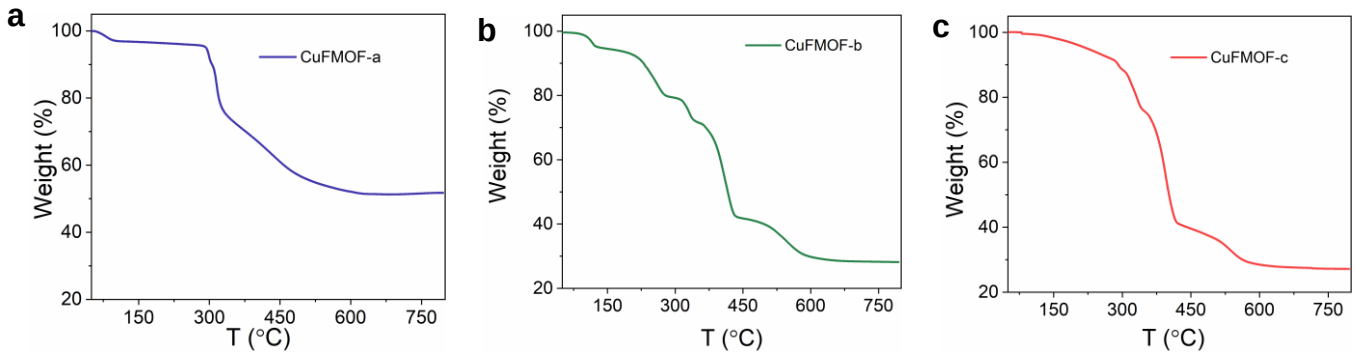

Fig. S6. TGA curves of (a) CuFMOF-a, (b) CuFMOF-b, and (c) CuFMOF-c.

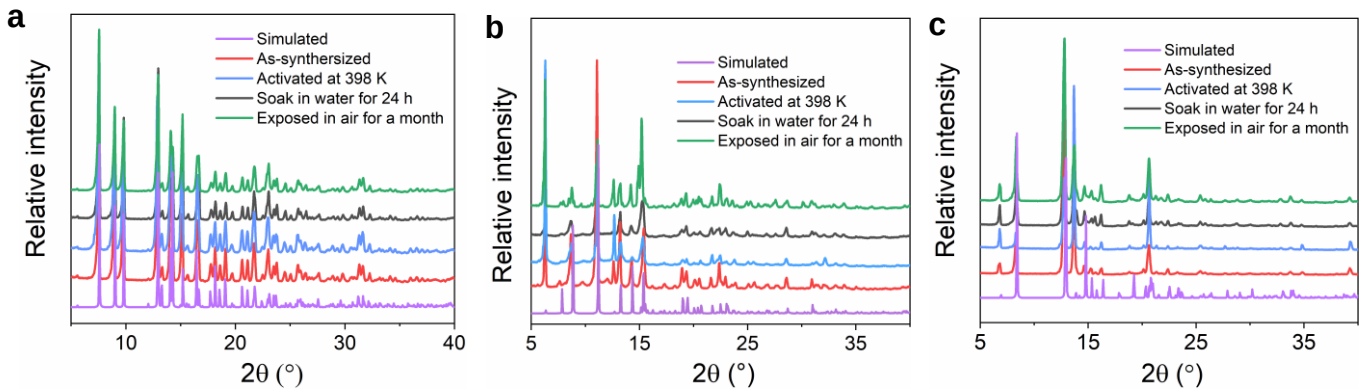

Fig. S7. PXRD patterns of MOFs and corresponding samples exposed to different conditions: (a) CuFMOF-a, (b) CuFMOF-b, and (c) CuFMOF-c.

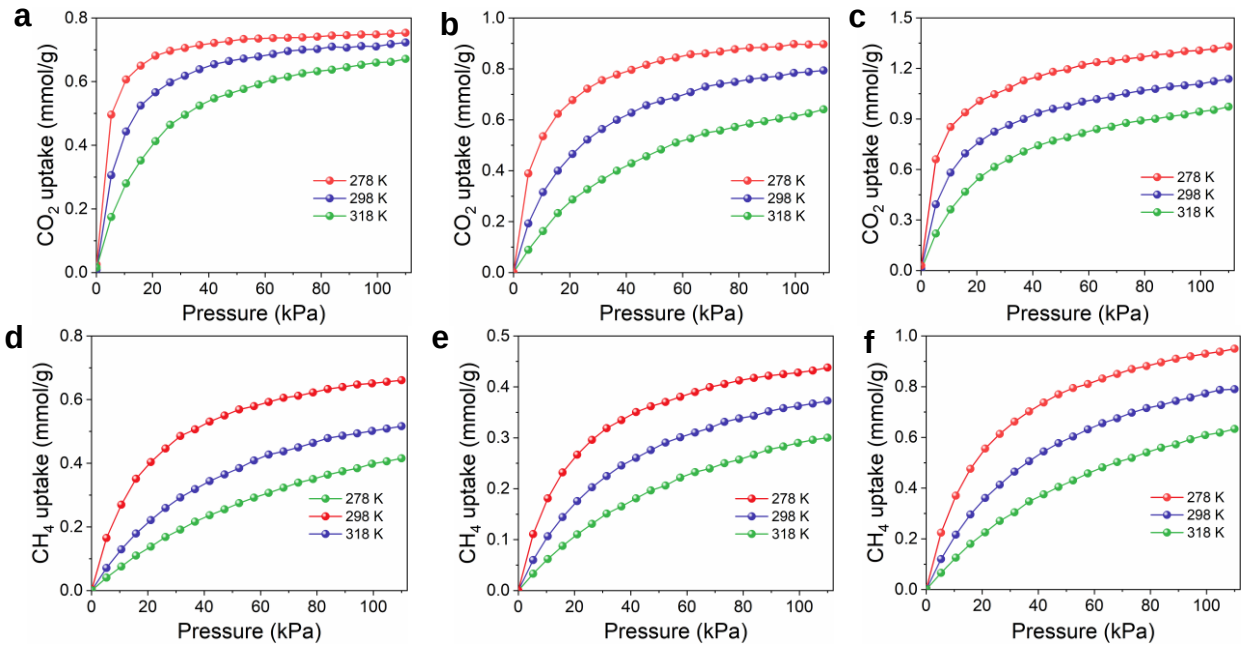

Fig. S8. The GCMC simulated single-component adsorption isotherms of CO_2 and CH_4 on (a, d) CuFMOF-a, (b, e) CuFMOF-c, and (c, f) CuFMOF-b at 278 K (green), 298 K (red) and 318 K (blue).

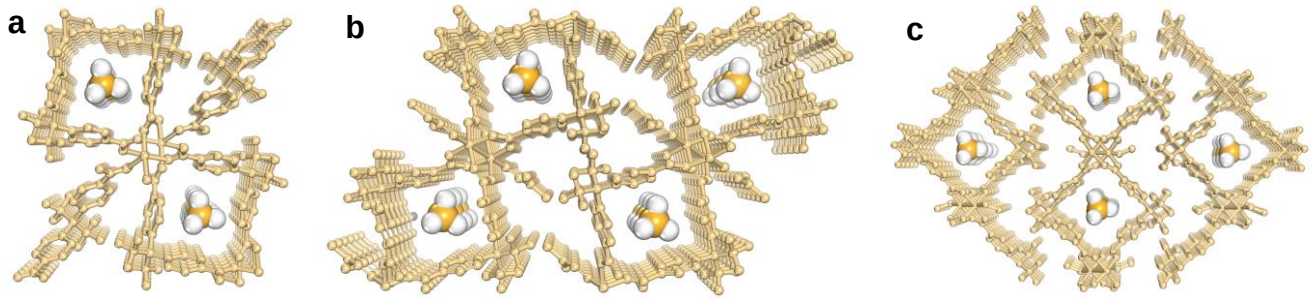

Fig. S9. Illustration of adsorbed methane molecule at the primary binding sites in (a) CuFMOF-a, (b) CuFMOF-b, and (c) CuFMOF-c as determined from simulation. The adsorption binding sites are located within the center cage space.

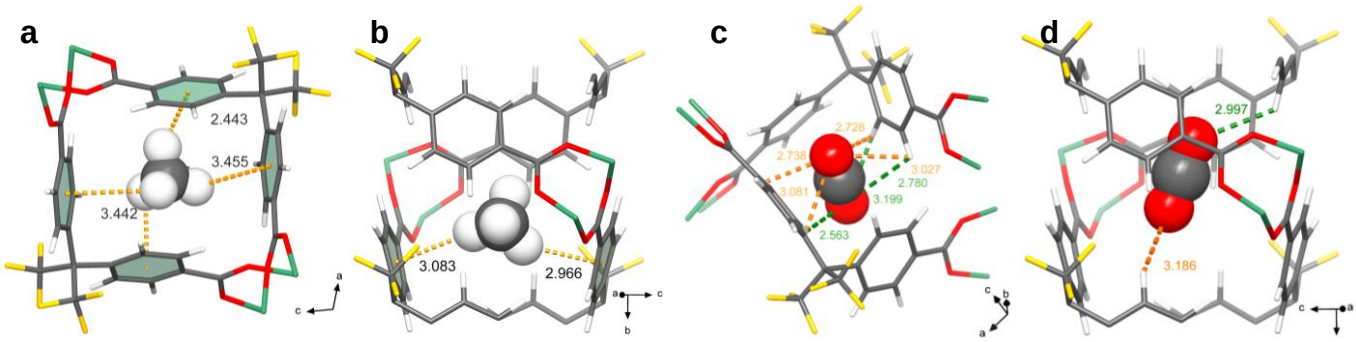

Fig. S10. MD calculated the minimum energy binding sites of (a, b) CH_4 and (c, d) CO_2 in the smallest bottleneck and the center of the capacious cages space of CuFMOF-a structure.

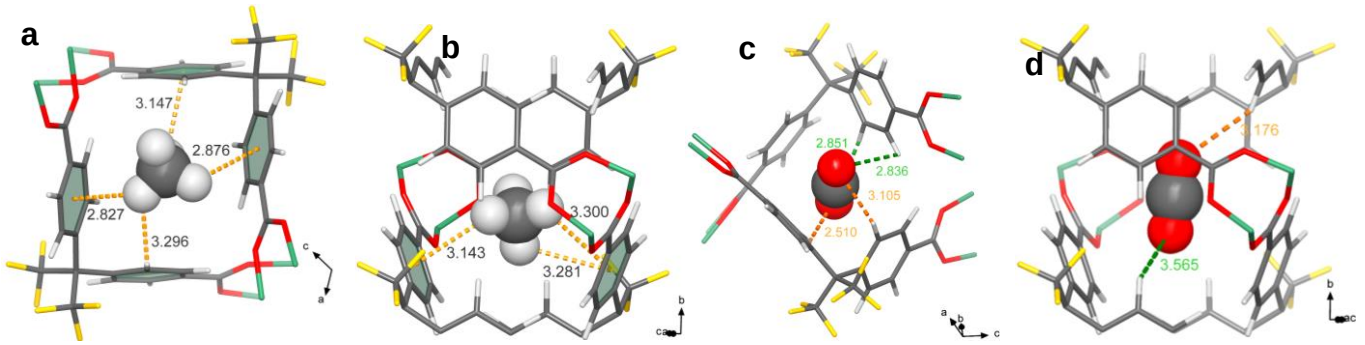

Fig. S11. MD calculated the minimum energy binding sites of (a, b) CH_4 and (c, d) CO_2 in the smallest neck bottle and the center of the capacious cages space of CuFMOF-b structure.

Table S1. Crystal data and structure refinement results for CuFMOF-a, CuFMOF-b, and CuFMOF-c.

Identification code	CuFMOF-a	CuFMOF-c	CuFMOF-b
Empirical formula	$C_{51}H_{26}Cu_2F_{18}O_{12}$	$C_{18}H_{12}CuF_6O_5$	$C_{20}H_{15}CuF_6NO_5$
Formula weight	1299.8	485.82	526.87
Temperature (K)	296.15	193	296.15
Crystal system	Monoclinic	Orthorhombic	Monoclinic
Space group	*P*12/*n*1	*Pccn*	*C*12/*c*1
Cell	*a* = 18.718 Å (8), *b* = 7.244 Å (3), *c* = 20.492 Å (9), *α* = 90°, *β* = 106.92°, *γ* = 90°	*a* = 25.6536 Å (8), *b* = 7.0064 Å (2), *c* = 22.9572 Å (7), *α* = 90°, *β* = 90°, *γ* = 90°	*a* = 32.088 Å (6), *b* = 7.299 Å (14), *c* = 22.996 Å (5), *α* = 90°, *β* = 120.05°, *γ* = 90°
Volume (Å^3)	2658.3(2)	4126.3(2)	4662.1(18)
Mu (mm^{-1})	0.924	6.198	1.014
D_c (g□cm^{-3})	1.624	1.564	1.501
Z	2	8	8
Reflns coll.	6114	3633	5391
Unique reflns	4177	2570	2632
R_{int}	0.0737	0.0596	0.0771
R_1 [$I > 2\sigma(I)$] [a]	0.0720	0.0560	0.0848
$wR_2[I > 2\sigma(I)]$ [b]	0.1191	0.1661	0.2449
R_1 (all data)	0.1179	0.0773	0.1555
wR_2 (all data)	0.1333	0.1876	0.2878
GOF	1.057	1.028	1.060

[a] $R_1 = \sum||F_o|-|F_c||/\sum|F_o|$.
[b] $wR_2 = [\sum w(F_o^2 - F_c^2)^2/\sum w(F_o^2)^2]^{1/2}$

Table S2. Crystal data and structure refinement results for activated CuFMOF-a, CuFMOF-b, and CuFMOF-c.

Identification code	CuFMOF-a	CuFMOF-c	CuFMOF-b
Empirical formula	$C_{51}H_{26}Cu_2F_{18}O_{12}$	$C_{18}H_{13}CuF_6O_5$	$C_{20}H_{15}CuF_6NO_5$
Formula weight	1299.8	486.82	526.87
Temperature (K)	193	173	193
Crystal system	Monoclinic	Monoclinic	Monoclinic
Space group	*P*12/*n*1	*C*2/*c*	*C*12/*c*1
Cell	*a* = 18.711 Å (10), *b* = 7.249 Å (4), *c* = 20.477 Å (11), *α* = 90°, *β* = 106.87°, *γ* = 90°	*a* = 28.073 Å (7), *b* = 7.005 Å (16), *c* = 23.086 Å (2), *α* = 90°, *β* = 114.63°, *γ* = 90°	*a* = 32.089 Å (3), *b* = 7.279 Å (6), *c* = 23.126 Å (19), *α* = 90°, *β* = 120.35°, *γ* = 90°
Volume (Å^3)	2657.8(3)	4127.4(6)	4661.3(8)

Identification code	CuFMOF-a	CuFMOF-c	CuFMOF-b
Mu (mm^{-1})	5.048	6.169	5.525
D_c (g/cm^3)	1.624	1.567	1.502
Z	2	8	8
reflns coll.	6104	3650	5306
unique reflns	4978	2752	2327
R_{int}	0.0715	0.0956	0.1051
R_1 [$I > 2\sigma(I)$][a]	0.0426	0.1011	0.0871
$wR_2[I > 2\sigma(I)]$[b]	0.1064	0.2205	0.2257
R_1 (all data)	0.0560	0.1227	0.1535
wR_2 (all data)	0.1115	0.2321	0.2821
GOF	1.083	1.143	0.936

[a] $R_1 = \sum||F_o|-|F_c||/\sum|F_o|$.
[b] $wR_2 = [\sum w(F_o^2 - F_c^2)^2/\sum w(F_o^2)^2]^{1/2}$

Table S3. Langmuir–Freundlich fit parameters for CO_2 and CH_4 for CuFMOF-a.

Adsorptive	T (K)	q_A ($mol \cdot kg^{-1}$)	b_A ($kPa^{-\nu A}$)	ν_A	R^2
CO_2	278	0.782	0.0764	1.1287	0.9999
	298	0.7867	0.0392	1.0189	0.9993
	318	0.7826	0.0193	1.0206	0.9999
CH_4	278	0.5318	0.0289	1.0043	0.9999
	298	0.5297	0.0100	1.0730	0.9999
	318	0.4538	0.0069	1.0653	0.9997

Table S4. Langmuir–Freundlich fit parameters for CO_2 and CH_4 for CuFMOF-b.

Adsorptive	T (K)	q_A ($mol \cdot kg^{-1}$)	b_A ($kPa^{-\nu A}$)	ν_A	R^2
CO_2	278	1.0041	0.0552	1.1317	0.9999
	298	0.9987	0.0301	1.0581	0.9999
	318	0.9895	0.01797	1.0052	0.9998
CH_4	278	0.8004	0.0266	0.9608	0.9999
	298	0.7857	0.0137	0.9835	0.9994
	318	0.6655	0.0089	0.9993	0.9997

Table S5. Langmuir–Freundlich fit parameters for CO_2 and CH_4 for CuFMOF-c.

Adsorptive	T (K)	q_A ($mol \cdot kg^{-1}$)	b_A ($kPa^{-\nu A}$)	ν_A	R^2
CO_2	278	1.1968	0.0819	1.2051	0.9998
	298	1.1685	0.02888	1.0614	0.9999
	318	1.1075	0.01745	1.0105	0.9996
CH_4	278	0.9233	0.0247	1.2758	0.9999
	298	1.0379	0.0132	0.918	0.9999
	318	0.9835	0.0074	0.9984	0.9999

Table S6. Diffusion time constants for of CO_2 and CH_4 and kinetic selectivity of CO_2/CH_4 in the activated CuFMOF-a, CuFMOF-c, and CuFMOF-b.

Material	T (K)	CH_4 D_C/r_c^2 $(10^{-5}\ s^{-1})$	CO_2 D_C/r_c^2 $(10^{-5}\ s^{-1})$	Kinetic selectivity CO_2/CH_4
CuFMOF-a	278	1.045	0.114	11.2
	298	1.215	0.195	16.1
	318	1.442	0.274	19.0
CuFMOF-c	278	0.606	1.657	273.5
	298	1.795	1.803	100.5
	318	4.034	2.030	50.3
CuFMOF-b	278	3.452	1.734	50.1
	298	7.312	2.645	36.1
	318	13.62	3.152	23.1

Table S7. Comparison of CO_2/CH_4 selectivity of different porous materials

Material	T (K)	Henry's selectivity	Kinetic selectivity	Equilibrium-kinetic combined selectivity
CuFMOF-a[a]	278	5.2	11.2	17.4
	298	5.0	16.1	20.1
	318	4.2	19	18.3
CuFMOF-c[a]	278	3.9	273.5	64.2
	298	2.9	100.5	29.1
	318	2.8	50.3	19.9
CuFMOF-b[a]	278	3.8	50.1	26.9
	298	3.2	36.1	19.2
	318	3.0	23.1	14.4
sOMC[b] [3]	278	36.1	0.60	21.8
CMS-3K[c] [4]	308	1.3	1.1	1.36
CMS-T3A[c] [5]	293	3.3	91.7	31.6
CMS-3A[c] [6]	343	2.8	537.3	64.9
BF-CMS[c] [6]	298	5.2	180	69.8
5A (Sinopec)[c] [7]	298	7.8	3.6	14.8

[a] Kinetic adsorption tests were performed on 10 kPa.
[b] Kinetic adsorption tests were performed on 2 kPa.
[c] Kinetic adsorption tests were performed on 100 kPa.
[d] Kinetic adsorption tests were performed on 800 torr.

Table S8. Diffusion activation energy of CO_2 and CH_4.

Adsorbent	CO_2 E_a (kJ· mol^{-1})	CH_4 E_a (kJ· mol^{-1})
CuFMOF-a	15.1	5.9
CuFMOF-b	10.3	24.2
CuFMOF-c	7.2	32.3

Table S9. Lennard–Jones (LJ) potential of CO_2 and CH_4.

Atom	LJ potential parameters		Charge	Type of force field
	ε/k_B (K)	σ (Å)		
$C(CO_2)$	28.129	2.757	+0.61	EPM2
$O(CO_2)$	80.507	3.033	-0.305	EPM2
$C(CH_4)$	147.0	3.730	0	TraPPE

Table S10. Langmuir fit parameters for CO_2 and CH_4 for CuFMOF-a.

Adsorptive	T (K)	$q_{A,sat}$ (mol·kg^{-1})	b_A (kPa^{-vA})	R^2
CO_2	278	0.8158	0.0940	0.9991
	298	0.7965	0.0404	0.9999
	318	0.7999	0.0199	0.9999
CH_4	278	0.5266	0.0282	0.9999
	298	0.5967	0.0108	0.9998
	318	0.5277	0.0072	0.9998

Table S11. Langmuir fit parameters for CO_2 and CH_4 for CuFMOF-b.

Adsorptive	T (K)	$q_{A,sat}$ (mol·kg^{-1})	b_A (kPa^{-vA})	R^2
CO_2	278	1.0569	0.0692	0.9993
	298	1.0422	0.0309	0.9998
	318	0.9959	0.01809	0.9999
CH_4	278	0.7694	0.0251	0.9999
	298	0.7650	0.0134	0.9994
	318	0.6644	0.0089	0.9997

Table S12. Langmuir fit parameters for CO_2 and CH_4 for CuFMOF-c.

Adsorptive	T (K)	$q_{A,sat}$ (mol·kg^{-1})	b_A (kPa^{-vA})	R^2
CO_2	278	1.1760	0.0769	0.9997
	298	1.2222	0.0319	0.9996
	318	1.1221	0.01769	0.9999
CH_4	278	0.9313	0.0250	0.9999
	298	1.0308	0.0132	0.9999
	318	0.9792	0.0074	0.9999

References

[1] Sheldrick GM. Phase Annealing in Shelx-90 - Direct Methods for Larger Structures, *Acta Crystallogr. A* 1990;46467-73.
[2] Ruthven DM, *Principles of adsorption and adsorption processes*, John Wiley & Sons, 1984.
[3] Yuan B, Wu XF, Chen YX, Huang JH, Luo HM, Deng SG, Adsorption of CO_2, CH_4, and N_2 on Ordered Mesoporous Carbon: Approach for Greenhouse Gases Capture and Biogas Upgrading, *Environ. Sci. Technol.* 2013;*47*(10):5474-80.
[4] Cavenati S, Grande CA, Rodrigues AE, Separation of $CH_4/CO_2/N_2$ mixtures by layered pressure swing adsorption for upgrade of natural gas, *Chem. Eng. Sci.* 2006;*61*(12):3893-906.
[5] Bae YS, Lee CH, Sorption kinetics of eight gases on a carbon molecular sieve at elevated pressure, *Carbon* 2005;*43*(1):95-107.
[6] Jayaraman A, Chiao AS, Padin J, Yang RT, Munson CL, Kinetic separation of methane/carbon dioxide by molecular sieve carbons, *Separ. Sci. Technol.* 2002;*37*(11):2505-28.
[7] Saha D, Bao ZB, Jia F, Deng SG, Adsorption of CO_2, CH_4, N_2O, and N_2 on MOF-5, MOF-177, and Zeolite 5A, *Environ. Sci. Technol.* 2010;*44*(5):1820-6.